

# Electronic Landscape of Ce-based Intermetallics: $\text{CeCu}_2\text{Si}_2$ at an Extreme

Y. Lai<sup>1,2</sup>, S. Saunders<sup>1,3</sup>, D. Graf<sup>1</sup>, A. Gallagher<sup>1,2</sup>, K.-W. Chen<sup>1,2</sup>, F. Kametani<sup>4</sup>, T. Besara<sup>1</sup>, T. Siegrist<sup>1</sup>, A. Shekhter<sup>1</sup>, R. E. Baumbach<sup>1,2\*</sup>

<sup>1</sup>*National High Magnetic Field Laboratory, Florida State University*

<sup>2</sup>*Department of Physics, Florida State University*

<sup>3</sup>*Iowa State University and the Ames Laboratory and*

<sup>4</sup>*Applied Superconductivity Center Florida State University*

(Dated: August 12, 2022)

## Abstract

The cerium based intermetallics that crystallize in the  $\text{ThCr}_2\text{Si}_2$ -type structure exhibit a multitude of exotic electronic states including magnetism, spin/charge instabilities, quantum criticality, and superconductivity. Although competition between the Kondo and RKKY energy scales captures some aspects of these phenomena, this does not immediately reveal the systematic trends in chemical composition series. Here we show that the nearly independent parameters of unit cell volume and  $d$ -shell filling of the transition metal element capture the major trends in the behavior throughout this entire family of compounds, where the locus of the exotic electronic states coincides with a crossover region between trivalent and intermediate valence  $f$ -electron states. Guided by this topography, we have studied  $\text{Si} \rightarrow \text{P}$  substitution ( $s/p$ -shell filling) and the effect of applied pressure in  $\text{CeCu}_2\text{Si}_2$ , which tunes the electronic behavior in a manner that is consistent with the proposed map. This result provides insight into the  $f$ -electron physics in this family of materials and renews the educated exploration of the chemical phase space.

---

\* To whom correspondence should be addressed. E-mail: baumbach@magnet.fsu.edu

## I. INTRODUCTION

Understanding magnetism, intermediate valence, unconventional superconductivity, and breakdown of Fermi liquid behavior in correlated electron materials is a persistent challenge. [1–7] For Ce-based  $f$ -electron lattices, most discussion relies on a model where the Kondo and RKKY interactions compete with each other to determine the ground state behavior. [8–12] While the Kondo interaction suppresses magnetism through screening of the  $f$ -electron moments by the conduction electrons, the RKKY interaction favors magnetic order by providing an exchange interaction between  $f$ -moments. Importantly, both interactions are mediated by the same wide band itinerant electrons which mostly originate on the  $s$ ,  $p$ , and  $d$  orbitals of the transition metal ions or ligand matrix. This scenario was described early-on in the Doniach phase diagram, [8] and since then a multitude of compounds have been characterized in this way; noteworthy examples include  $\text{CeTIn}_5$  ( $T = \text{Co, Rh, Ir}$ ) [13, 14] and  $\text{CeT}_2\text{X}_2$  ( $T = \text{transition metal and } X = \text{Si, Ge}$ ). [15, 16] Although this picture has proved useful to qualitatively understand these families of materials, efforts to develop it into a quantitative model have been challenged by the inherent complexity of the correlated electron problem; even the task of calculating the band structure for a cerium based metal remains difficult. Also missing is an understanding of how and where spin and charge instabilities play a role. To confront these issues, we adapt the Kondo vs. RKKY scenario to a chemical perspective by examining a simplified parameterization of the known Ce-based materials within the  $\text{ThCr}_2\text{Si}_2$ -type structure using their unit cell volume and  $d$ -shell filling of the transition metal element. In this topography, the magnetic and non-magnetic members are well separated and the crossover between these regions is populated by those examples that exhibit non-Fermi liquid behavior and unconventional superconductivity. While this picture captures only the major characteristics of these materials, it organizes their phenomena in a simple way that provides an educated path forward.

Here we focus on  $\text{CeCu}_2\text{Si}_2$  because it is located at maximum  $d$ -shell filling and has close-to the smallest unit cell volume of the naturally occurring 122 analogues. It will be shown that it occupies a special position in the 2D map.  $\text{CeCu}_2\text{Si}_2$  exhibits a rich variety of behaviors including spin density wave magnetism, breakdown of the Fermi liquid, possible quantum criticality, and unconventional superconductivity. [17–23] Of particular interest is that it hosts a second superconducting dome at high pressure, which might be associated

with an  $f$ -electron valence change quantum phase transition. [22, 24–26] The maximum superconducting transition temperature in this region is twice that of the low-pressure antiferromagnetic quantum phase transition, which suggests a strengthened superconducting pairing mechanism. We investigated the chemical substitution series  $\text{CeCu}_2(\text{Si}_{1-x}\text{P}_x)_2$  which simultaneously decreases the unit cell volume and fills the  $s/p$  shells of the ligand site, in analogy to  $d$ -shell filling. We find that the superconductivity is rapidly suppressed and is replaced by strengthening magnetism with increasing  $x$ . To probe the influence of further unit cell contraction, we carried out measurements under applied pressure, where magnetism is suppressed and superconductivity is recovered at a quantum phase transition for lightly substituted samples. These results are consistent with expectations from our map, reveal its usefulness for controlling the  $f$ -electron phenomena of Ce-based materials in the  $\text{ThCr}_2\text{Si}_2$  structure, and help to plot a course to bring the intriguing high pressure behavior of  $\text{CeCu}_2\text{Si}_2$  to ambient conditions.

## II. RESULTS

While there has been substantial work on  $\text{Ce}T_2X_2$  ( $T$  = transition metal and  $X$  = Si and Ge) and related compounds seeking to unravel their physics using tuning parameters such as applied pressure and chemical substitution, [17–21, 23, 27–31] it remains challenging to arbitrarily induce behavior such as unconventional superconductivity. This is because most tuning strategies explore a non-trivial vector amongst the various factors that control the strongly correlated  $f$ -electron metallic state. Here, we propose that this is addressed for Ce-based materials with the  $\text{ThCr}_2\text{Si}_2$ -type structure by organizing them in the two-dimensional map shown in Fig. 1, where the axes are unit cell volume ( $\Delta V$ ) and  $d$ -shell filling ( $x$ ). Similar proposals have previously been made, [32–35] but they mostly do not consider current knowledge about spin/charge instabilities and how they relate to quantum criticality. Thus, it is useful to reexamine the chemical topography of such  $f$ -electron materials with renewed attention paid to the importance of spin and charge fluctuations in critical regions.

The isoelectronic subset where  $T$  = Cu, Ag, Au and  $X$  = Si, Ge illustrates the distinct effect of the unit cell volume, where these materials show strengthening of antiferromagnetism with increasing unit cell volume. [15, 16] Notably this antiferromagnetism is suppressed with

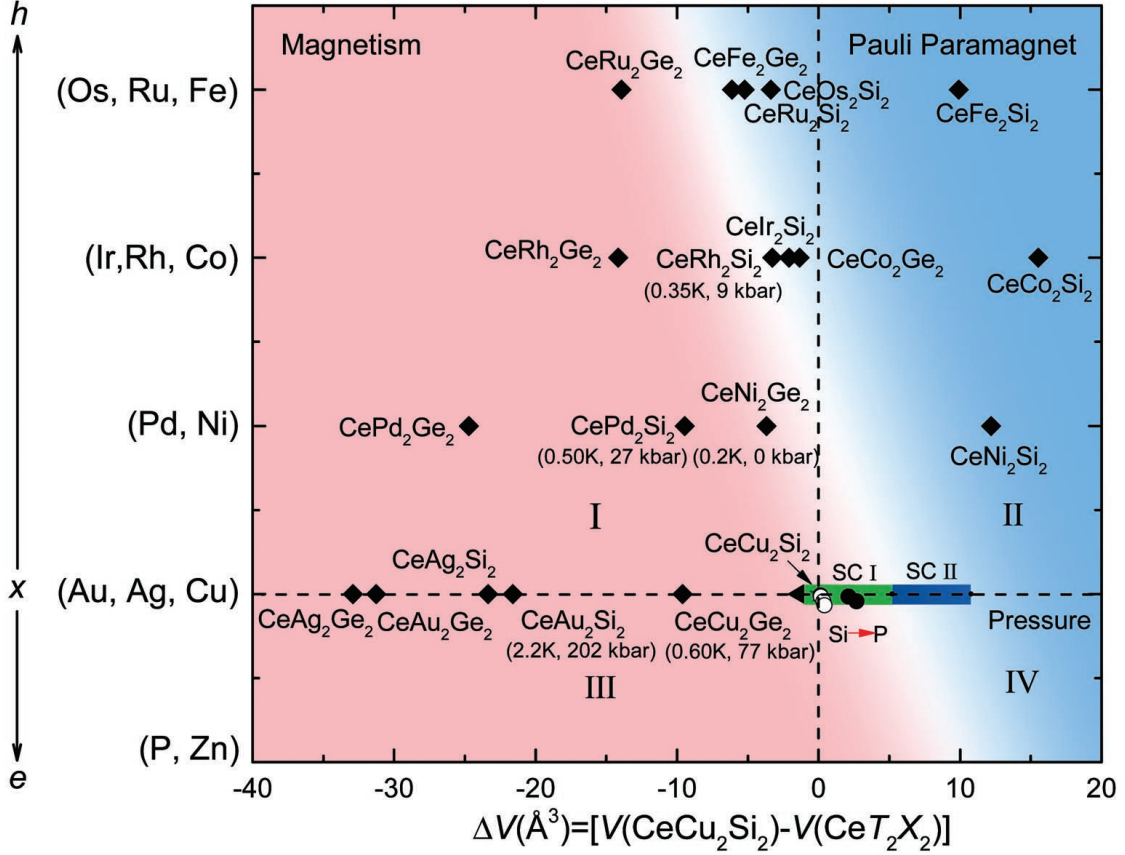


FIG. 1. Phase diagram for the compounds  $\text{CeT}_2\text{X}_2$  ( $T$  = transition metal and  $X = \text{Si}, \text{Ge}$ ) that crystallize in the  $\text{ThCr}_2\text{Si}_2$ -type structure. [15, 16] The axes that define the four quadrants (I-IV) and control the ground state behavior are the difference in unit cell volume ( $\Delta V$ ) from that of  $\text{CeCu}_2\text{Si}_2$  and increasing  $d$ -shell filling going from the Fe column to the Cu column ( $x$ ). The white band that traverses the center of the phase diagram approximately separates the magnetic (left hand side) and intermediate valence examples (right hand side). The bars labeled SC1 (green) and SC2 (dark blue) show the regions where superconductivity is observed for  $\text{CeCu}_2\text{Si}_2$  along the  $\Delta V$  axis. [17–21, 23] In parenthesis are the maximum superconducting transition temperatures that are observed under applied pressure for those compounds with an antiferromagnetic quantum phase transition. [20, 21, 27–31] In quadrant IV the open circles show the zero temperature magnetic phase boundary resulting from the investigation of the substitution series  $\text{CeCu}_2(\text{Si}_{1-x}\text{P}_x)_2$  presented here (see Fig. 3). The closed circles show where applied pressure suppresses magnetic ordering to quantum phase transitions in this series (see Fig. 4).

applied pressure, with a return of superconductivity at the magnetic quantum phase transition. [20, 21, 30, 31] A similar relationship between magnetism and unit cell volume is seen for the other isoelectronic series ( $T = \text{Ni, Pd}$  and  $X = \text{Si, Ge}$ ), ( $T = \text{Co, Rh}$  and  $X = \text{Si, Ge}$ ), and ( $T = \text{Fe, Ru, Os}$  and  $X = \text{Si, Ge}$ ) [15, 16] and related trends are broadly seen in other Ce-based intermetallics, as is expected in the Doniach picture. [3–7] The effect of non-isoelectronic tuning is less transparent, but is clarified by considering the examples along the vertical axis with similar unit cell volumes: e.g., those extending from  $\text{CeCu}_2\text{Si}_2 \rightarrow \text{CeNi}_2\text{Ge}_2 \rightarrow \text{CeCo}_2\text{Ge}_2 \rightarrow \text{CeFe}_2\text{Ge}_2$  all show strong  $f$ - and conduction electron hybridization with no ordered ground state for  $T = \text{Ni, Co, and Fe}$ . Importantly, the  $f$ -electron valence  $v$  tends to increase from  $v = 3$  towards  $v \approx 3 + \Delta$  between  $\text{Cu} \rightarrow$  half  $d$ -shell filling, after which it again decreases towards  $v = 3$ . [32] This indicates that the hybridization strength is maximized between the Fe and Co columns. A consequence of the relationship between these two distinct axes is that there exists a region that separates the magnetic and nonmagnetic members, where extensive work has shown that clustered along it are those systems that exhibit exotic metallic states, magnetic quantum phase transitions and superconductivity. [15, 16, 20, 21, 27–29, 31] It is important to note that this picture does not account explicitly for some factors that might sometimes play an important role: e.g., the influences of (1) chemical disorder and (2) differences between  $3d$ ,  $4d$ , and  $5d$  orbitals. Nonetheless, it captures the global trends in this family.

This topography immediately suggests that  $\text{CeCu}_2\text{Si}_2$  is located not only in the crossover region, but also near the unit cell volume and  $d$ -shell filling extremal point. It is appealing to infer that its unique behavior derives from this position in the proposed phase space, as is indicated by many tuning studies. Most notably, while negative pressure ( $\text{Si} \rightarrow \text{Ge}$ ) stabilizes magnetism, decreasing the  $d$ -shell filling ( $\text{Cu} \rightarrow \text{Ni}$ ) or applied pressure induce two distinct domes of superconductivity [36, 37] that may connect through a partial annulus in quadrant II (Fig. 2). This uncovers a systematic way to access the regions that host unconventional superconductivity and non-Fermi-liquid behavior in  $\text{CeCu}_2\text{Si}_2$ , where a straightforward strategy is to investigate increasing shell filling. Thus motivated, we synthesized the series  $\text{CeCu}_2(\text{Si}_{1-x}\text{P}_x)_2$  for  $x \lesssim 0.1$ , where X-ray diffraction measurements reveal that  $\text{Si} \rightarrow \text{P}$  substitution results in a continuous isostructural contraction of the unit cell volume, yielding a chemical pressure with a maximum  $P_{\text{chem}} \approx 5$  kbar at  $x \approx 0.1$  (Fig. 3a). In a naive picture for a generic cerium Kondo lattice it is expected that decreasing unit cell

volume will increase the hybridization strength and destabilize the magnetism by driving the  $f$ -electron valence from 3+ towards 4+: e.g., as seen in exemplary families of materials such as  $\text{CeTIn}_5$  ( $T = \text{Co, Rh, In}$ ) and  $\text{CeCu}_{6-x}\text{Au}_x$ . [3–7] We instead find that  $\text{Si} \rightarrow \text{P}$  substitution weakens the hybridization between the  $f$ - and conduction electrons (e.g., as evidenced by a decreasing Kondo coherence temperature  $T_{\text{coh}}$ ), rapidly suppresses the parent compound superconductivity, and induces complex magnetism (Figs. 2 and 3). This is consistent with our expectation from Fig. 1 that the  $f$ -electron physics depends strongly not only on the unit cell volume but also shell filling.

The  $f$ -electron behavior in this chemical substitution series is uncovered in more detail by considering the magnetic susceptibility ( $\chi = M/H$ ), electrical resistivity ( $\rho$ ), and heat capacity divided by temperature ( $C/T$ ) at several concentrations  $x = 0 - 0.1$  (Figs. 3 and S2-5). Particularly noteworthy is that the magnetism becomes more anisotropic with increasing  $x$ , as evidenced by the strengthening  $\chi(T)$  for  $H \parallel c$  that yields a nearly tenfold increase in the low temperature magnetic anisotropy between  $x = 0 - 0.1$ . Curie-Weiss fits to  $\chi(T)$  for  $H \parallel c$  further show that the effective magnetic moment  $\mu_{\text{eff}} \approx 2.5 - 2.6 \mu_{\text{B}}/\text{Ce}$  remains nearly constant and the Curie-Weiss temperature  $\Theta$  decreases with  $x$ , eventually becoming positive near  $x \approx 0.08$ . This shows that while phosphorous substitution controls the magnetocrystalline anisotropy, it does not drive the trivalent cerium towards an intermediate valence. A complex evolution of the magnetic ground state is also observed, where the low  $x$  normal state behavior signals the onset of ‘A-phase’ antiferromagnetism, as seen in self-doped  $\text{CeCu}_2\text{Si}_2$  and  $\text{CeCu}_2(\text{S}_{1-x}\text{Ge}_x)_2$  [18, 19]: i.e.,  $\rho$  and  $C/T$  exhibit a weak kink and lambda-anomalies at  $T_{\text{A}}$ , respectively. Near  $x \approx 0.03 - 0.04$ , the kink in  $\rho(T)$  is replaced by an abrupt reduction in the resistivity at  $T_{\text{N}}$  that appears in  $C/T$  as a broadened lambda-like anomaly and  $\chi(T)$  as a broad decrease near  $T_{\text{N}} = 2.1 \text{ K}$ , suggesting that the nature of the magnetic ordering changes near this concentration.  $T_{\text{N}}$  subsequently sharpens and moves to higher  $T$  with increasing  $x$ . Near  $x \approx 0.06$  a second small hysteretic increase in  $\chi$  appears at  $T_{\text{C}} < T_{\text{N}}$ , consistent with a spin reconfiguration with a ferromagnetic component. The phase transition at  $T_{\text{C}}$  is also seen in  $\rho(T)$  and  $C/T$ , is reflected in the sign change of  $\Theta$  near this concentration, and evolves under an applied magnetic field as expected for an ordered state with ferromagnetic character (Fig. S6). This phase diagram is notably similar to that of  $\text{CeCu}_2(\text{S}_{1-x}\text{Ge}_x)_2$ , [18, 19] revealing the smooth connection between increasing unit cell volume and shell filling.

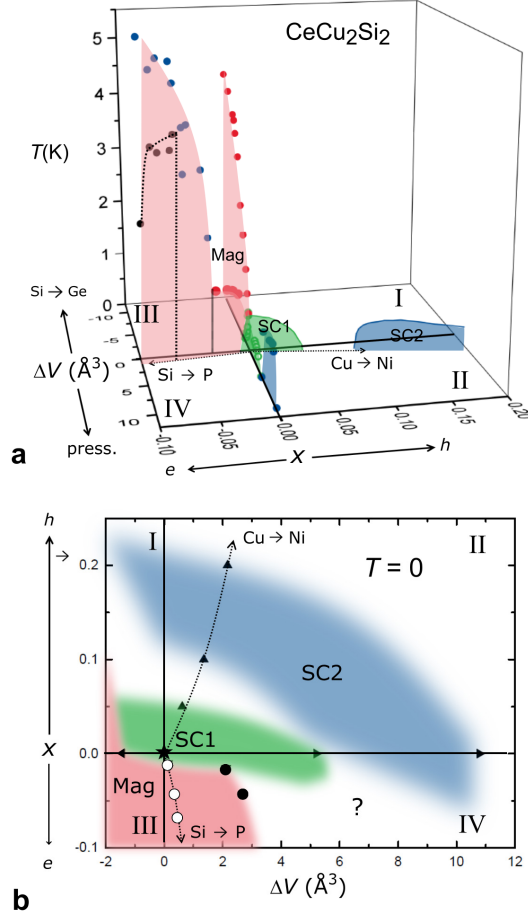


FIG. 2. **Phase diagram in the vicinity of  $\text{CeCu}_2\text{Si}_2$**  (a) Combined temperature ( $T$ ) - difference in unit cell volume, compared to that of  $\text{CeCu}_2\text{Si}_2$  ( $\Delta V$ ) - shell filling ( $x$ ) phase diagram showing magnetism (Mag) and two superconducting regions (SC1 and SC2) in the phase space close to  $\text{CeCu}_2\text{Si}_2$ . Data points for Si  $\rightarrow$  Ge substitution, [18, 19] applied pressure, [20, 21] and Cu  $\rightarrow$  Ni substitution, [36, 37] are taken from the literature. Phase boundaries for the the Si  $\rightarrow$  P substitution series are from data presented here (see Fig. 3). (b) The zero temperature projection of the  $T - \Delta V - x$  phase diagram close to  $\text{CeCu}_2\text{Si}_2$ . The solid triangles represent phase boundaries seen in Si  $\rightarrow$  Ge substitution, applied pressure, and Cu  $\rightarrow$  Ni substitution studies. The open white circles show the superconducting and magnetic phase boundaries that are identified in the Si  $\rightarrow$  P substitution series presented here (see Fig. 3). The closed circles show where applied pressure suppresses magnetic ordering to quantum phase transitions in this series (see Fig. 4).

In order to further examine the scenario presented in Figs. 1 and 2, where independent decrease of the unit cell volume is expected to strengthen the electronic hybridization, we

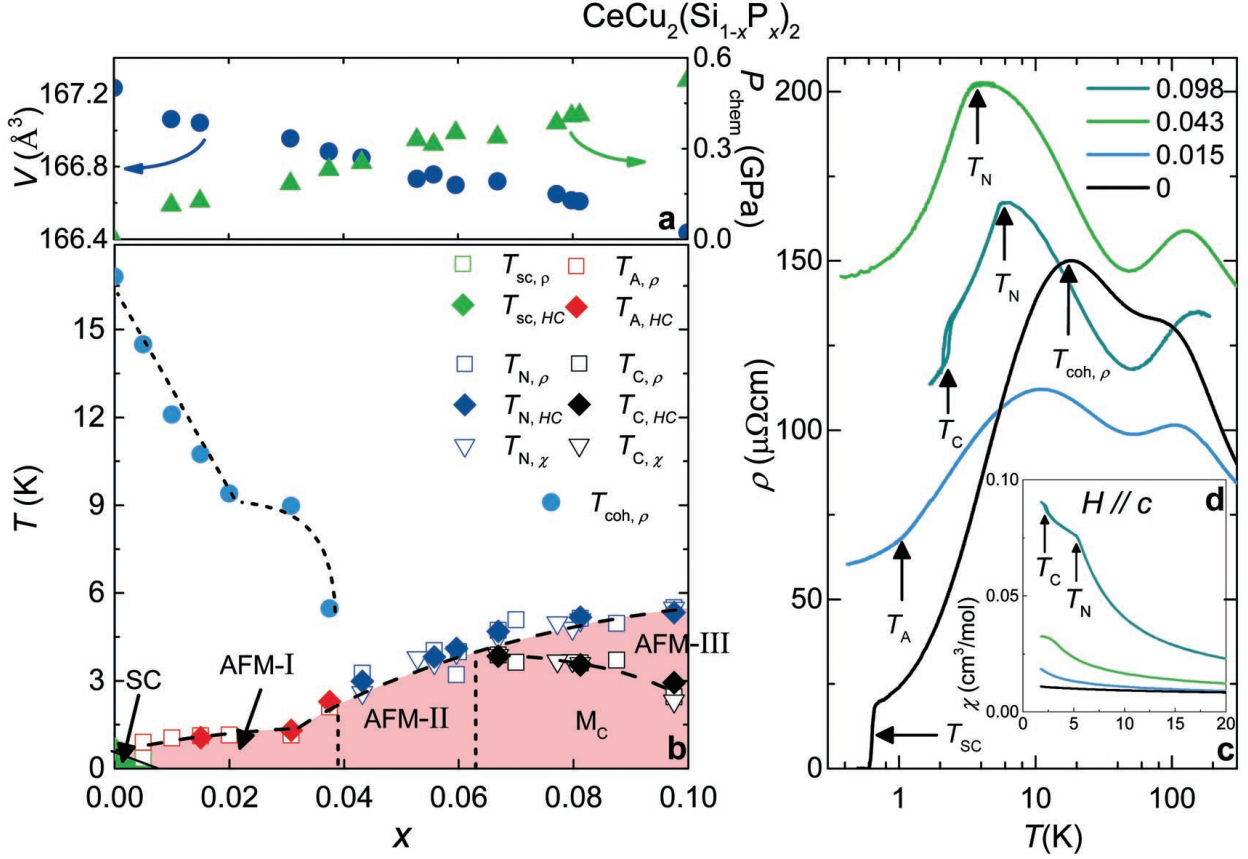


FIG. 3. Summary of thermodynamic and electrical transport results for  $\text{CeCu}_2(\text{Si}_{1-x}\text{P}_x)_2$  at concentrations  $x = 0 - 0.1$ . (a) Unit cell volume  $V$  (left axis) and chemical pressure  $P_{\text{chem}}$  vs.  $x$ , where  $x$  is the measured value (see Fig. S1a).  $P_{\text{chem}}$  was obtained using the Birch-Murnaghan equation of state, as described in the supplementary section. (b) Temperature  $T$  - phosphorous concentration  $x$  phase diagram for  $\text{CeCu}_2(\text{Si}_{1-x}\text{P}_x)_2$  constructed from magnetic susceptibility  $\chi$ , heat capacity  $C$ , and electrical resistivity  $\rho$  vs.  $T$  measurements. The magnetic ordering temperatures  $T_{\text{A}}$ ,  $T_{\text{N}}$ , and  $T_{\text{C}}$  are defined as shown in Fig. S2. Detailed plots of these quantities are shown in Figs. S3-5. The coherence temperature  $T_{\text{coh}}$  appears as a broad hump in  $\rho(T)$ . (c)  $\rho$  vs.  $T$  for select values of  $x$  in representative parts of the  $T - x$  phase diagram. (d)  $\chi$  vs.  $T$  for magnetic field  $H = 0.5$  T applied parallel  $\parallel$  to the  $c$ -axis for representative  $x$ .

performed measurements of the electrical resistivity under hydrostatic pressures for select concentrations ( $x = 0.015, 0.043, 0.098$ ) spanning  $T - x$  phase diagram (Fig. 4). For  $x = 0.015$  and  $0.045$ , both  $T_{\text{A}}$  and  $T_{\text{N}}$  are suppressed with initial slopes  $\partial T_{\text{A}}/\partial P = 0.06$  K/kbar and  $\partial T_{\text{N}}/\partial P = 0.07$  K/kbar and are extrapolated to approach zero temperature near  $P_{\text{c}} \approx$



12 – 16 and 18 – 22 kbar, respectively. Near  $P = 15$  kbar for  $x = 0.015$ , superconductivity is recovered with an onset temperature  $T_{\text{SC}} \approx 150$  mK and the normal state electrical resistivity follows the temperature dependence  $\rho(T) = \rho_0 + AT^n$  where  $n \approx 1.16$  (Figs. 4b inset and S7), indicating a departure from Fermi liquid behavior. The superconductivity is noticeably robust against disorder, which is revealed here in the large residual resistivity. We further note that for both of these concentrations,  $T_{\text{coh}}$  increases with increasing  $P$ , as is expected upon strengthening the hybridization between the  $f$  - and conduction electrons. For  $x = 0.098$ , both magnetic ordering temperatures  $T_{\text{N}}$  and  $T_{\text{C}}$  are suppressed by pressure with slopes  $\partial T_{\text{N}}/\partial P = 0.06$  K/kbar and  $\partial T_{\text{C}}/\partial P = 0.1$  K/kbar, where the extrapolated critical pressures are above 20 kbar.

### III. DISCUSSION

These results unify earlier work and suggest strategies for how to promote behavior such as the high pressure (dome 2) superconductivity in  $\text{CeCu}_2\text{Si}_2$  at ambient pressure. For instance, simultaneous doping on both the transition metal and ligand sites,  $\text{Cu} \rightarrow \text{Ni}$  &  $\text{Si} \rightarrow \text{P}$ , such that their combined effect would be pure unit cell contraction is of interest. However, an important obstacle is chemical disorder, which typically suppresses superconductivity in these materials. [27–29] An alternative route is to consider electronic tuning in examples that are close to  $\text{CeCu}_2\text{Si}_2$  but on the right hand side of the magnetic phase boundary seen in Fig. 1. For instance,  $\text{CeNi}_2\text{Ge}_2$  already exhibits non-Fermi-liquid behavior and incipient superconductivity, [28] suggesting that small  $\text{Ge} \rightarrow \text{P}$  or  $\text{As}$  substitution might stabilize bulk superconductivity. We further note that the unstable valence physics and superconductivity extends into quadrant 4, as demonstrated through our applied pressure study. This is the least studied region of the phase diagram and its investigation will give insight into the interesting region surrounding  $\text{CeCu}_2\text{Si}_2$  and has the potential to produce unexpected discoveries.

We further point out that our map helps to organize the factors that distinguish individual materials from each other. For instance, while  $\text{CeRu}_2\text{Si}_2$  is nearly quantum critical, [4, 38] it does not exhibit superconductivity. In contrast, the pressure driven antiferromagnetic quantum critical points that are seen for  $\text{CeRh}_2\text{Si}_2$  and  $\text{CePd}_2\text{Si}_2$  are surrounded by superconducting domes where the Cooper pairing is thought to be mediated by spin fluctuations.[3–

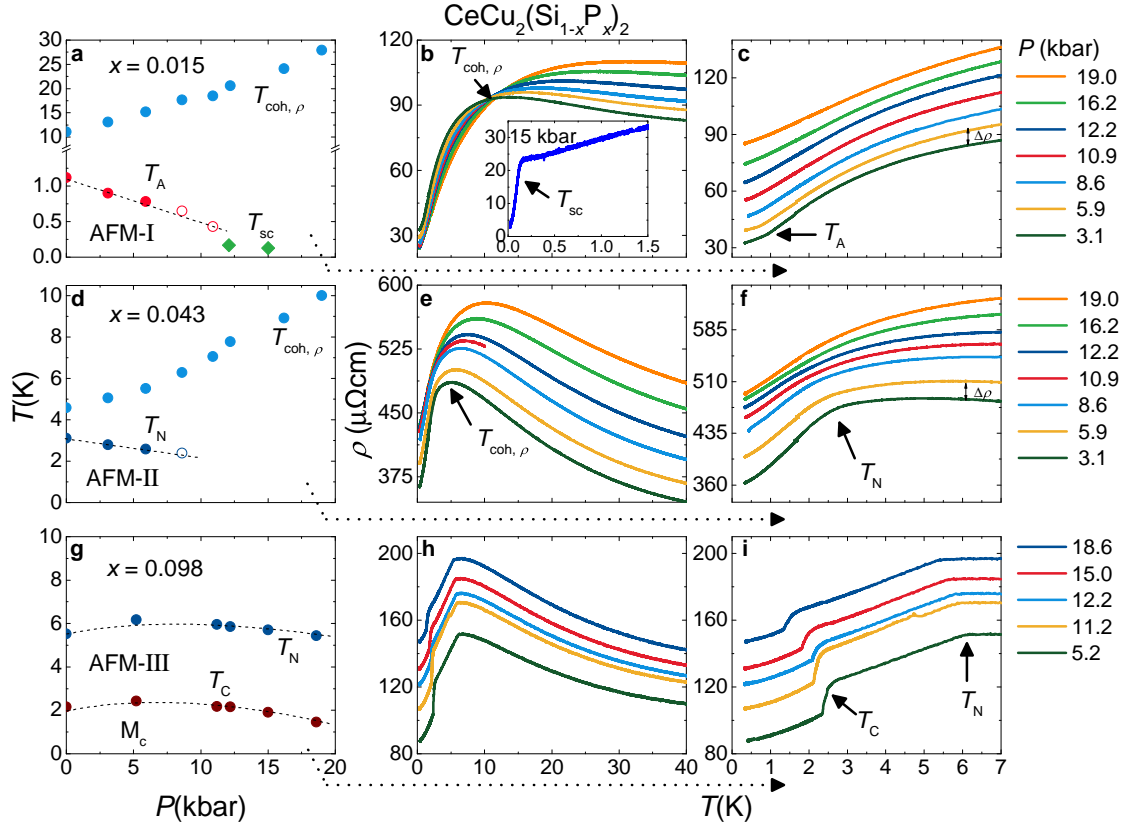


FIG. 4. **Summary of electrical resistivity  $\rho$  vs. temperature  $T$  measurements under applied pressure  $P$  for  $\text{CeCu}_2(\text{Si}_{1-x}\text{P}_x)_2$  at select concentrations  $x = 0.015$ ,  $0.043$ , and  $0.098$ .** The magnetic ordering temperatures  $T_A$ ,  $T_N$ , and  $T_C$  are defined as shown in Fig. S2. For clarity, the curves for  $x = 0.015$  and  $0.043$  are offset by constant values  $\Delta\rho = 10 \mu\Omega\text{cm}$ . (a) Temperature  $T$  - pressure  $P$  phase diagram for  $x = 0.015$  for  $P < 20$  kbar showing the suppression of  $T_A$ , the enhancement of  $T_{\text{coh}}$ , and the appearance of superconductivity at the extrapolated quantum phase transition. Open circles indicate ambiguity in defining  $T_A$ . (b)  $\rho(T)$  for  $x = 0.015$  for  $P < 20$  kbar at  $0 < T < 40$  K where the Kondo coherence temperature  $T_{\text{coh}}$  appears as a broad hump. (c)  $\rho(T)$  for  $x = 0.015$  for pressures  $P < 20$  kbar and  $0 < T < 7$  K. (d)  $T$  -  $P$  phase diagram for  $x = 0.043$  for  $P < 20$  kbar. (e)  $\rho(T)$  for  $x = 0.043$  for  $P < 20$  kbar at  $0 < T < 40$  K. (f)  $\rho(T)$  for  $x = 0.043$  for pressures  $P < 20$  kbar at  $0 < T < 7$  K. (g)  $T$  -  $P$  phase diagram for  $x = 0.098$  for several pressures  $P < 20$  kbar. (h)  $\rho(T)$  for  $x = 0.098$  for several pressures  $P$  and  $0 < T < 40$  K. (i)  $\rho(T)$  for  $x = 0.098$  at  $P < 20$  kbar and  $0 < T < 7$  K.

7, 27–29] This difference likely originates from the trends in the hybridization strength, which peaks near half filling of the  $d$ -shell. [32] This motivates the question of whether or not  $s/p$ -shell ligand-site filling should be viewed as simple charge doping, or if there might be trends that emerge with half-filling in this channel. For instance, in  $\text{CeIn}_{3-x}\text{Sn}_x$  the filling of the  $p$ -shell results in strengthening hybridization (despite an increasing unit cell volume) which might be expected to go through a maximum if it were possible to further dope the system (e.g., by introducing antimony). [39] We have so-far been unable to go beyond  $x \approx 0.1$  in the  $\text{Si} \rightarrow \text{P}$  series, but it is tempting to consider other ligand site tuning strategies. There also are several compounds with the formula  $\text{CeT}_2\text{Pn}_2$  ( $\text{Pn} = \text{P}, \text{As}$ ) which would be useful to probe in this way. [40–42] Another important feature is that within the nearly  $d$ -shell filled subset ( $T = \text{Cu}, \text{Ag}, \text{Au}$ ) there is rich superconducting behavior. While the high pressure superconductivity of  $\text{CeCu}_2\text{Si}_2$  involves an  $f$ -electron valence instability, [17–26] the high pressure superconductivity in  $\text{CeAu}_2\text{Si}_2$  coexists with (and may be enhanced by) magnetism.[31] This is an example of how variation from  $3d \rightarrow 5d$  electrons impacts behavior. From this, it is tempting to speculate that replacing Si or Ge with heavier  $p$ -block elements might enhance the superconductivity.

Finally, as shown in Fig. S8, similar maps also inform navigation amongst other  $f$ -electron containing 122 families of materials. For instance, it is immediately clear that although Pr and Sm sometimes exhibit unstable valence in other structures, there are no such regions that are easily accessed in the 122 structure. This makes it unappealing to consider these examples for further study. In contrast, both Yb- and Eu- based 122 compounds follow trends similar to that seen for Ce-based examples, while for the U-based examples the region that separates the magnetic and nonmagnetic regions is nearly horizontal. We further expect that future work will expose chemical trends in the numerous other families of materials that are derived from the  $\text{BaAl}_4$  structural building block (e.g.,  $\text{CaBe}_2\text{Ge}_2$ ,  $\text{CeNiSi}_2$ ,  $\text{ZrCuSi}_2$ ,  $\text{BaNiSn}_3$ ,  $\text{LuNi}_2\text{B}_2\text{C}$ , and  $\text{U}_2\text{Co}_3\text{Si}_5$ ). [43, 44] Taken together, these results greatly inform the exploration of chemical space of correlated  $f$ -electron materials, providing a step towards the goal of designing specific behavior - rather than serendipitously discovering it.

## IV. CONCLUSIONS

We have presented a model independent organizing principle for the Ce-based compounds that crystallize in the  $\text{ThCr}_2\text{Si}_2$ -type structure, which provides insight into which specific examples are expected to exhibit magnetism, unstable  $f$ -electron valence, non-Fermi liquid behavior, superconductivity, and intermediate valence behavior. The exemplary correlated electron superconductor  $\text{CeCu}_2\text{Si}_2$  is located at a nearly extremal position of naturally occurring relatives in this phase space.  $\text{Si} \rightarrow \text{P}$  chemical substitution and applied pressure reveal a complex phase diagram that smoothly connects to other tuning strategies in the vicinity of  $\text{CeCu}_2\text{Si}_2$  and based on this result, chemical strategies to access the valence-quantum criticality at zero pressure are proposed.

## V. ACKNOWLEDGEMENTS

This work was performed at the National High Magnetic Field Laboratory (NHMFL), which is supported by National Science Foundation Cooperative Agreement No. DMR-1157490, the State of Florida and the DOE.” A portion of this work was supported by the NHMFL User Collaboration Grant Program (UCGP). S. M. Saunders acknowledges support from the NHMFL REU program. We thank Z. Fisk and M. Janoschek for insightful discussions.

## VI. EXPERIMENTAL METHODS

Single crystals of  $\text{CeCu}_2\text{Si}_{2-x}\text{P}_x$  were grown from elements with purities  $> 99.9\%$  in a molten flux of Cu and Si. The reaction ampoules were prepared by loading the elements in the ratio  $\text{Ce}:\text{Cu}:\text{Si}:\text{P} ; 1:28:(11.44-x):x$  into a 2 mL alumina crucible for each of the different nominal dopings of P. The crucibles were sealed under vacuum in quartz ampoules and heated to  $600^\circ\text{C}$  at a rate of  $50^\circ\text{C}/\text{hour}$ , held at  $600^\circ\text{C}$  for 6 hours, heated to  $1185^\circ\text{C}$  at a rate of  $50^\circ\text{C}/\text{hour}$ , kept at  $1185^\circ\text{C}$  for 12 hours, and then cooled at a rate of  $2^\circ\text{C}/\text{hour}$  to  $940^\circ\text{C}$ . At this temperature, the remaining flux was separated from the crystals by centrifuging. Single-crystal platelets with typical dimensions of several millimeters on a side and several millimeters in thickness were collected.

The crystal structure and chemical composition were verified by single-crystal x-ray-diffraction (XRD) and energy dispersive spectrometer (EDS) analysis. A comparison between the nominal  $x_{\text{nom}}$  and actual  $x_{\text{act}}$  values is shown in Fig. S1. Throughout the manuscript,  $x$  refers to the measured value. Magnetization  $M(T, H)$  measurements were carried out for single crystals at temperatures  $T = 1.8 - 300$  K under an applied magnetic field of  $H = 5$  kOe for  $H$  applied both parallel ( $\parallel$ ) and perpendicular ( $\perp$ ) to the  $c$  axis using a Quantum Design VSM Magnetic Property Measurement System. Electrical resistivity  $\rho$  measurements for temperatures  $T = 0.5 - 300$  K and magnetic fields  $H = 0 - 9$  T were performed in a four-wire configuration and the heat capacity  $C$  was measured for  $T = 0.39 - 20$  K using a Quantum Design Physical Property Measurement System. Measurements under applied pressure were performed using a piston cylinder pressure cell with the pressure transmitting medium Daphne 7474 oil. The pressure is determined by the shift in ruby fluorescence peaks and are the values determined below  $T = 10$  K. These measurements were performed at the National High Magnetic Field Laboratory DC field User facility using standard He3 cryostats.

# Supplementary A: Electronic Landscape of Ce-based Intermetallics: $\text{CeCu}_2\text{Si}_2$ at an Extreme

## 1. Chemical analysis and X-ray diffraction

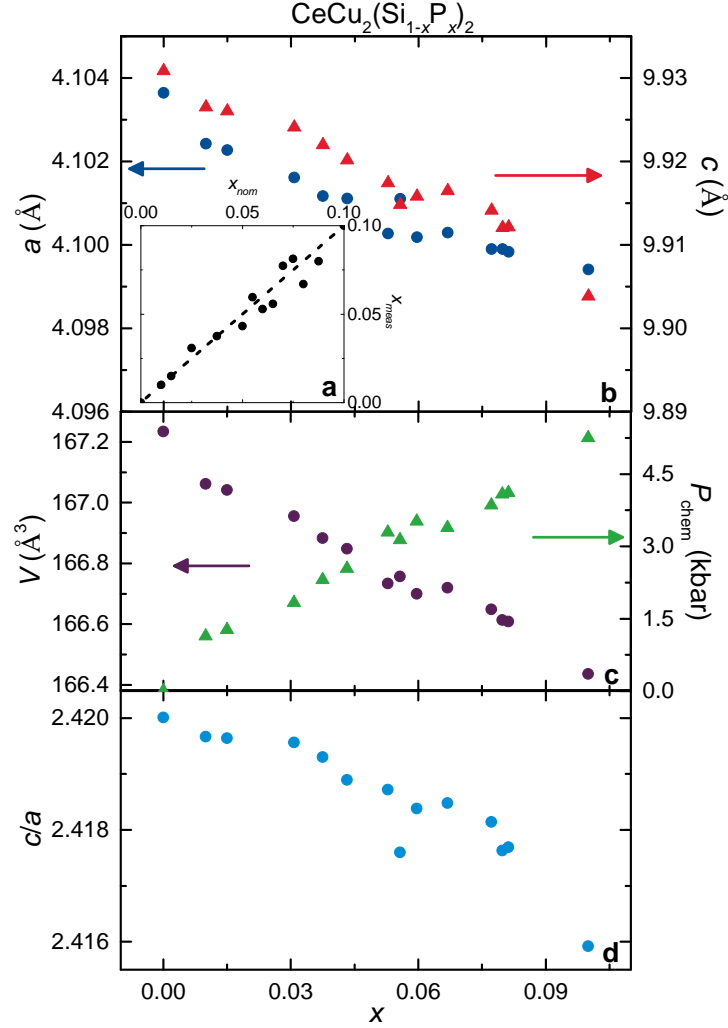


FIG. S1. (a) Comparison between the measured phosphorous concentration  $x_{\text{meas}}$  and the nominal concentration  $x_{\text{nom}}$ , where  $x_{\text{meas}}$  was determined using energy dispersive spectrometer analysis. Throughout the manuscript we use  $x_{\text{meas}} = x$  unless otherwise specified. (c) The lattice constants,  $a(x)$  (left axis) and  $c(x)$  (right axis). (b) the unit cell volume  $V(x)$  (left axis) and chemical pressure  $P_{\text{ch}}$  (right axis), calculated using the Burch-Murnaghan equation, where  $B_0 = 110$  GPa. [45] (d) the ratio  $c/a$  vs.  $x$ .

## 2. Identification of the ordering temperatures

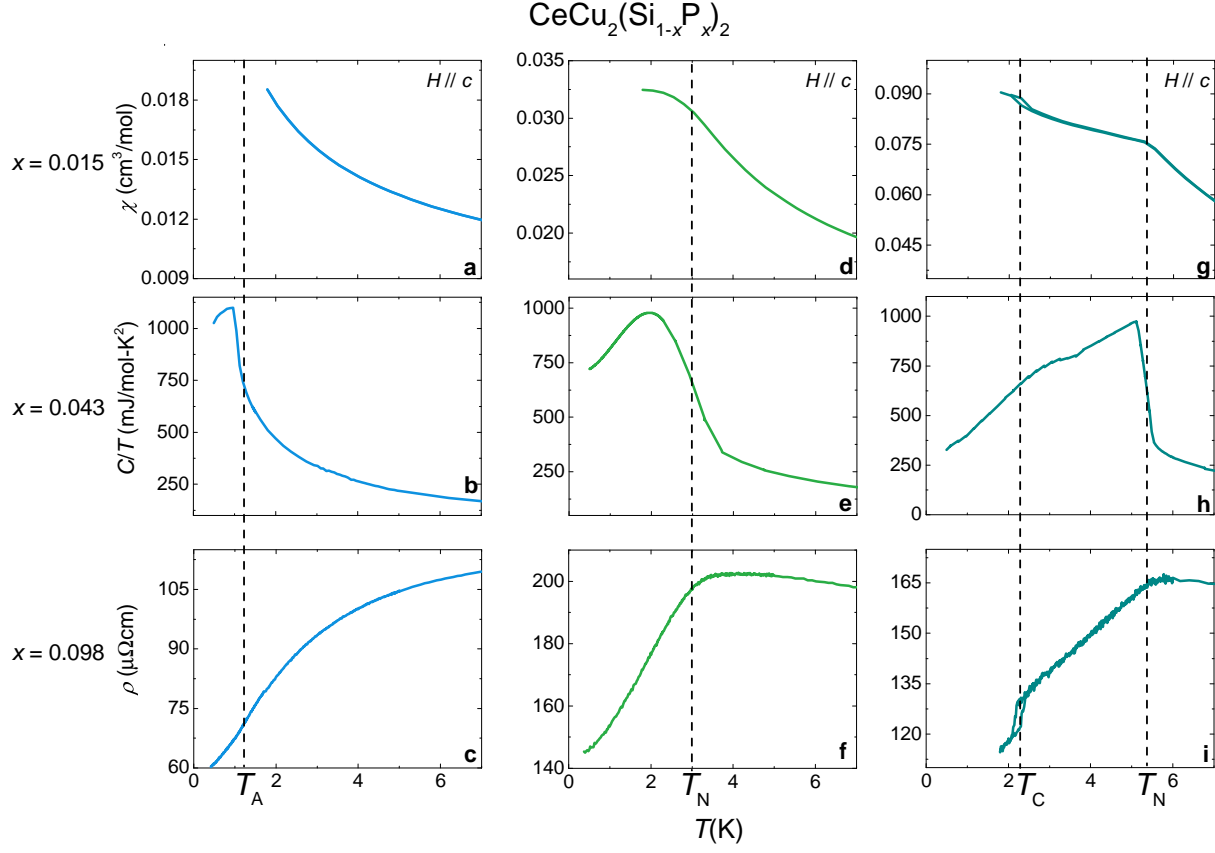


FIG. S2. Magnetic susceptibility  $\chi = M/H$ , heat capacity divided by temperature  $C/T$ , and electrical resistivity vs. temperature for select concentrations  $x = 0.015$ ,  $0.043$ , and  $0.098$  in regions I-III as described in the main text. The dotted lines denote the ordering temperatures  $T_A$ ,  $T_N$ , and  $T_C$ .  $T_A$  is defined as midpoint of the strong upturn in  $C/T$ . It also appears as a weak kink in  $\rho(T)$ .  $T_N$  is defined as the midpoint of the lambda-type transition in  $C/T$ . It also appears as a shoulder in  $\chi(T)$  and as a downturn in  $\rho(T)$ .  $T_C$  is a weak feature in  $C/T$ . Therefore, we define it as the midpoint of the hysteretic feature in  $\chi(T)$  and  $\rho(T)$ . There is good agreement in the values of  $T_A$ ,  $T_N$ , and  $T_C$  as determined from all three measurements.

### 3. Magnetic Susceptibility

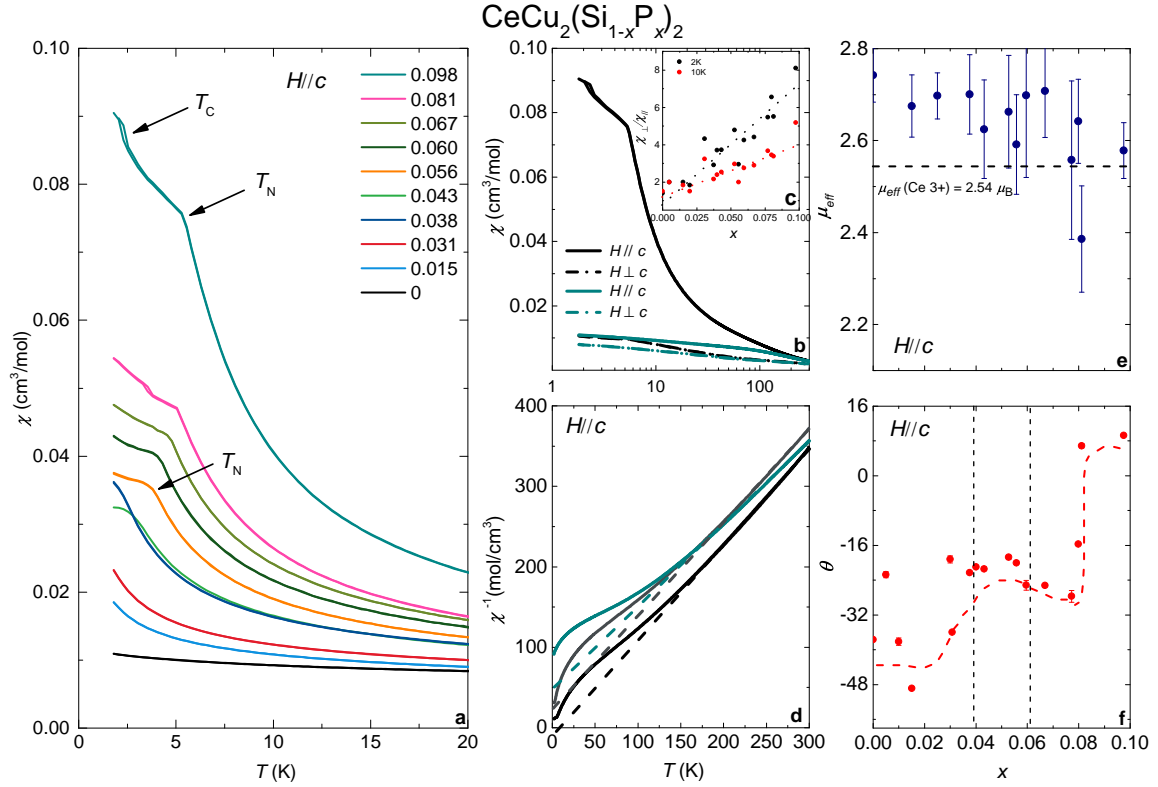


FIG. S3. (a) Magnetic susceptibility  $\chi = M/H$  collected in a magnetic field  $H = 5$  kOe applied  $\parallel$  to the  $c$ -axis of  $\text{CeCu}_2(\text{Si}_{1-x}\text{P}_x)_2$  for  $x = 0 - 0.1$ . (b) Magnetic susceptibility  $\chi$  vs. temperature  $T$  for  $\text{CeCu}_2(\text{Si}_{1-x}\text{P}_x)_2$  at select concentrations  $x = 0$  and  $0.098$  for magnetic fields  $H$  applied parallel  $\parallel$  (solid line) and perpendicular  $\perp$  (dotted line) to the  $c$ -axis. (c) The ratio of the magnetic susceptibilities for  $H \parallel$  and  $\perp$  to the  $c$ -axis at  $T = 2$  and  $10$  K vs.  $x$ . (d) The inverse magnetic susceptibility  $\chi^{-1}$  vs  $T$  for  $H \parallel c$  at concentrations  $x = 0, 0.043$ , and  $0.098$ . The dotted lines are Curie-Weiss fits to the data using the expression  $\chi(T) = C/(T-\Theta)$ . (e) The effective magnetic moment  $\mu_{\text{eff}}$  extracted from Curie-Weiss fits to  $\chi(T)$  vs.  $x$ . (f) The Curie-Weiss temperature  $\theta$  extracted from fits to  $\chi(T)$  vs.  $x$ .



#### 4. Heat capacity and 4f entropy

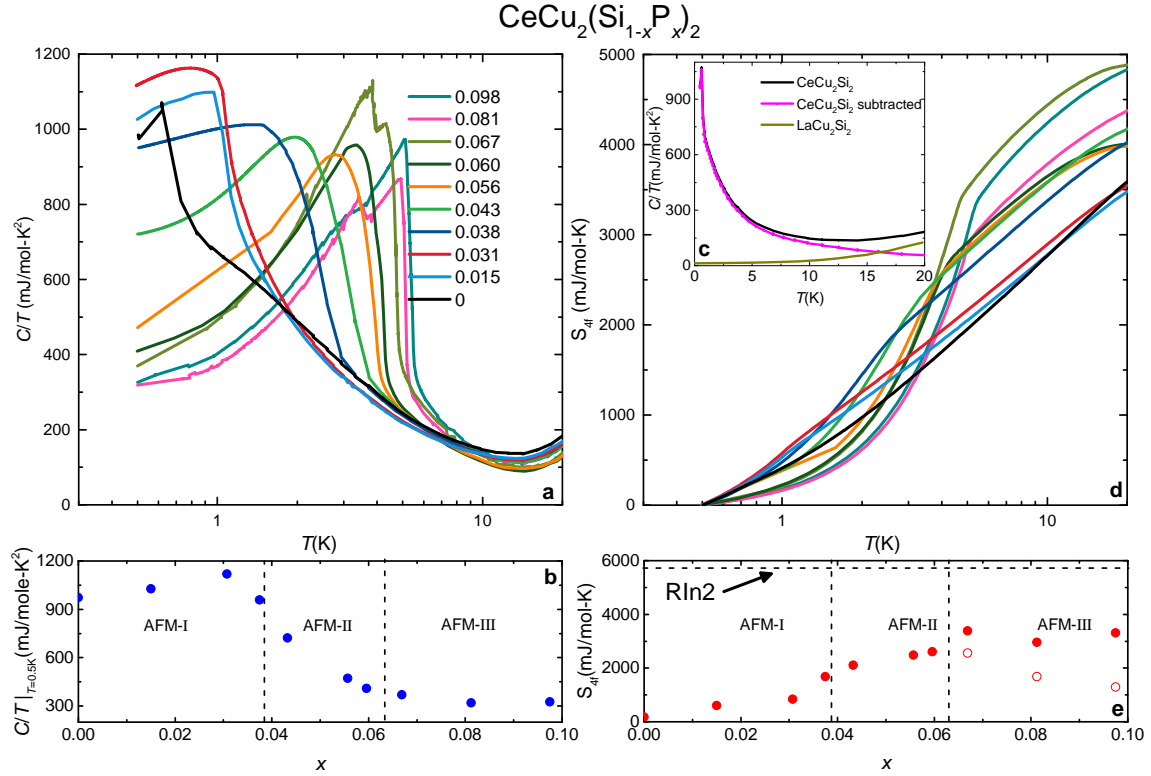


FIG. S4. (a) Heat capacity  $C$  divided by temperature  $T$  vs.  $T$  of  $\text{CeCu}_2(\text{Si}_{1-x}\text{P}_x)_2$  for  $x = 0 - 0.1$ . (b)  $C/T = \gamma$  obtained at  $T = 0.5$  K vs.  $x$ . (c)  $C/T$  vs.  $T$  for  $\text{CeCu}_2\text{Si}_2$  and  $\text{LaCu}_2\text{Si}_2$ . Also shown is the 4f contribution to the heat capacity of  $\text{CeCu}_2\text{Si}_2$  (blue circles)  $C_{4f}/T$ , which was acquired by subtracting the La contribution from that of the Ce compound. (d) The 4f contribution to the entropy  $S_{4f}$  vs.  $T$  for  $\text{CeCu}_2(\text{Si}_{1-x}\text{P}_x)_2$ .  $S_{4f}$  was acquired following the subtraction of  $C/T$  for  $\text{LaCu}_2\text{Si}_2$  from the chemically substituted specimens and subsequently integrating  $C_{4f}/T$  from  $T = 400$  mK. While this procedure underestimates  $S_{4f}$ , it provides a systematic approach to compare this quantity between concentrations. (e)  $S_{4f}$  at the ordering temperature vs.  $x$ .

## 5. Electrical Resistivity

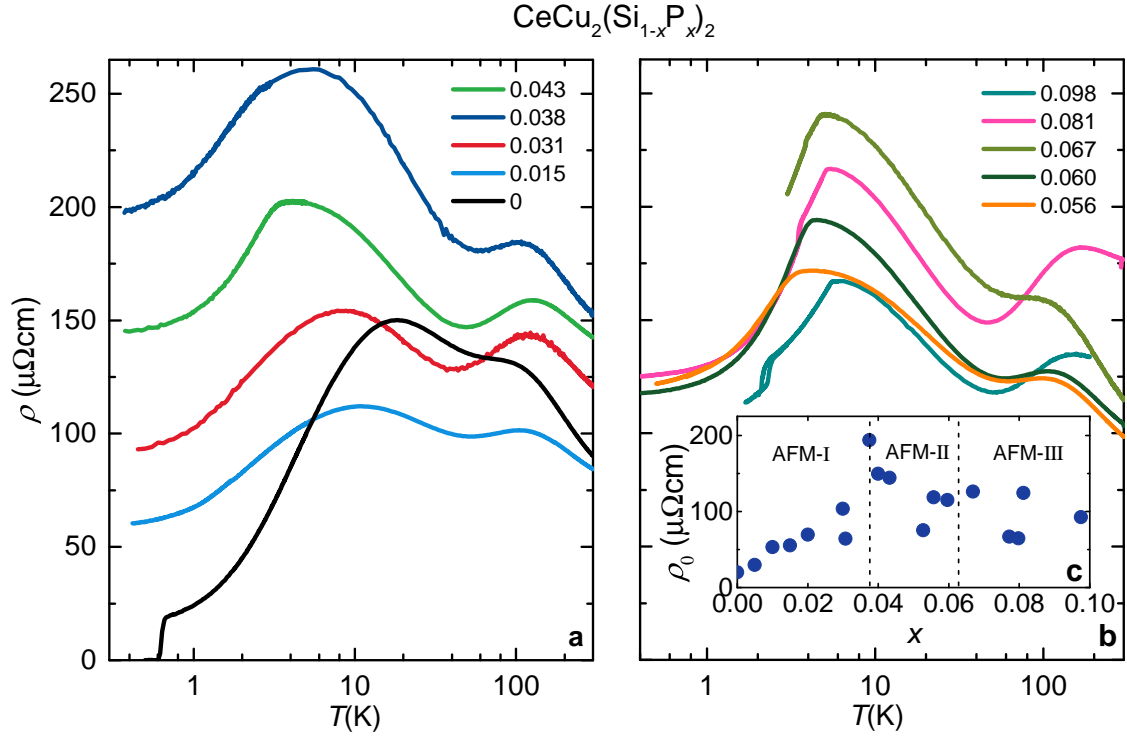


FIG. S5. (a) The electrical resistivity  $\rho$  vs.  $T$  for  $0 < x < 0.043$ . (b)  $\rho$  vs.  $T$  for  $0.056 < x < 0.098$ . (c) Residual resistivity  $\rho_0$  vs.  $x$ .

6. Evolution of the ordered state under applied magnetic field in regions III and III'

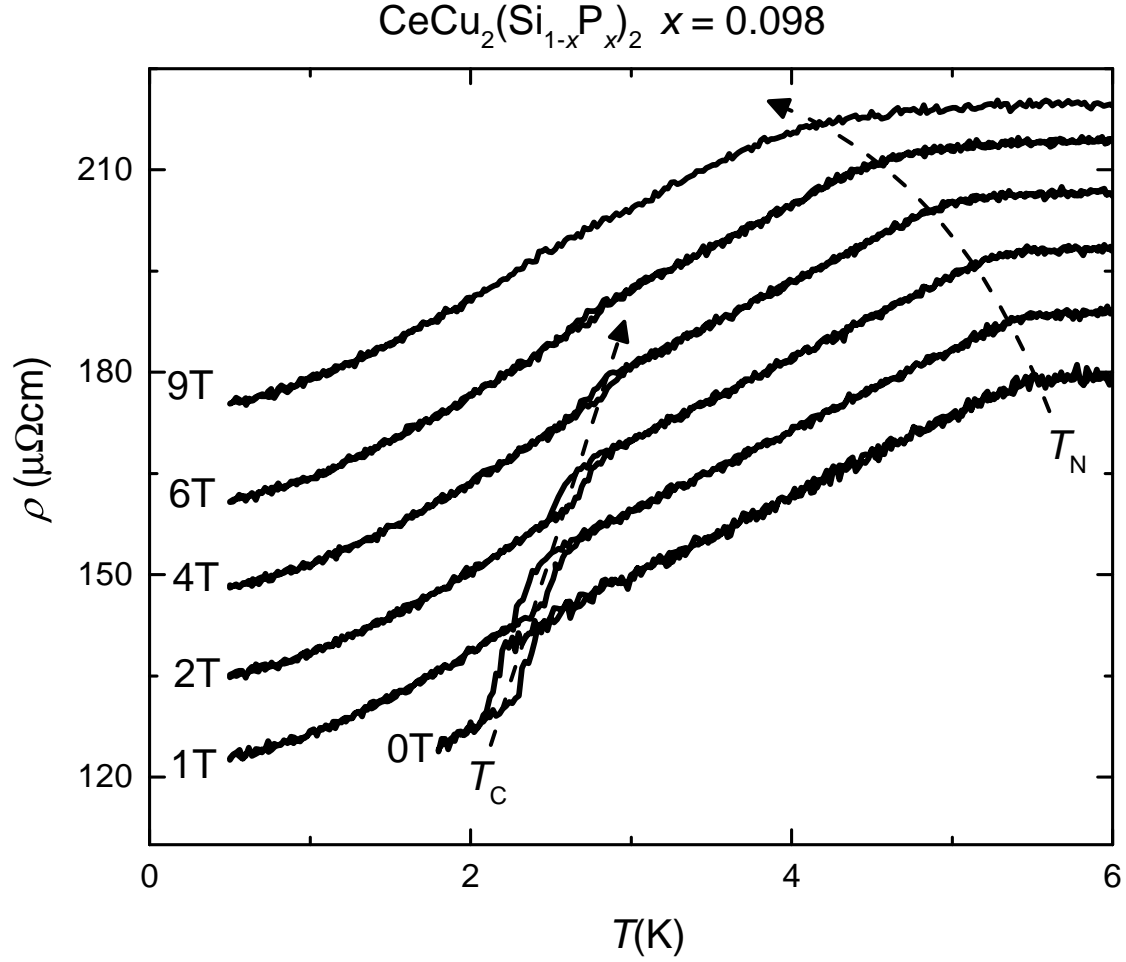


FIG. S6. Electrical resistivity  $\rho$  vs. temperature  $T$  in several magnetic fields  $H \leq 9\text{T}$ . The evolution of the Néel temperature  $T_N$  and the ferromagnet-like transition temperature  $T_C$  are indicated by dotted lines.

7. Electrical resistivity, superconductivity, and non-Fermi-liquid powerlaw behavior

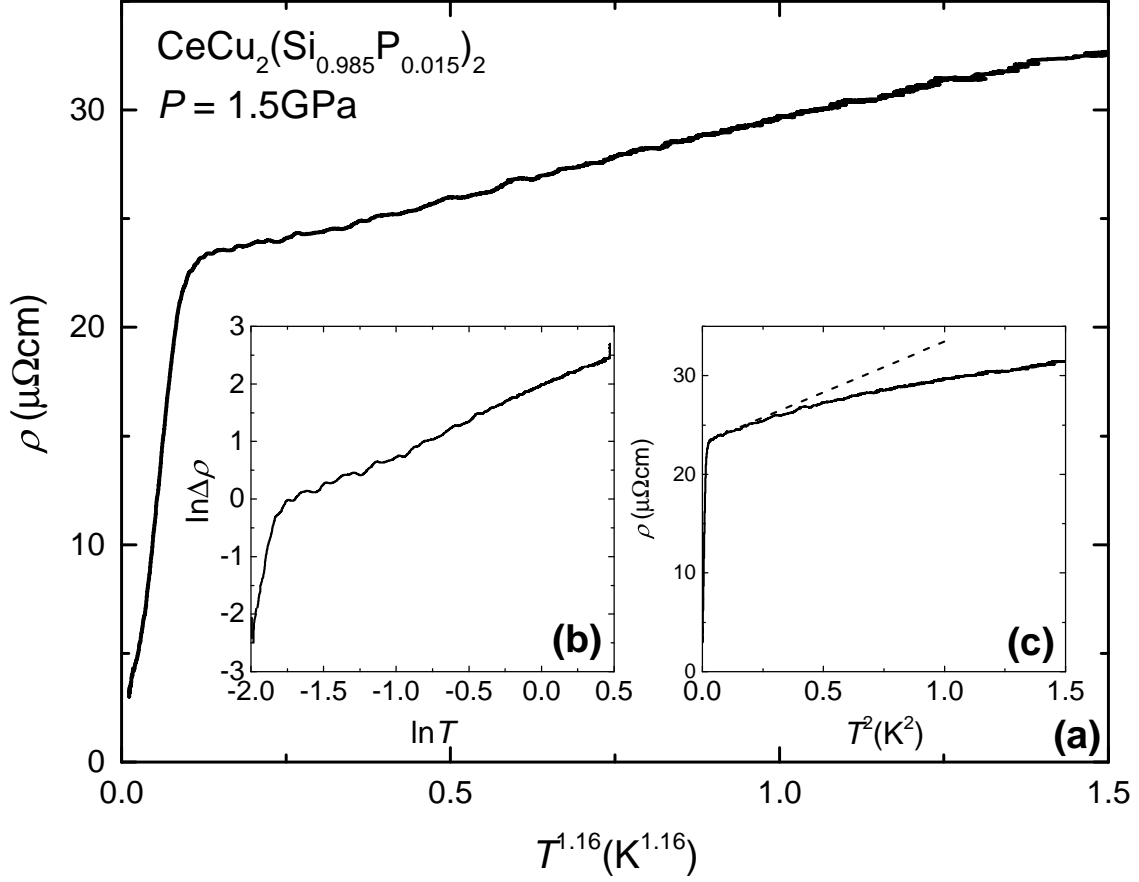


FIG. S7. (a) The electrical resistivity  $\rho$  vs. temperature  $T^{1.16}$  for  $\text{CeCu}_2(\text{Si}_{1-x}\text{P}_x)_2$  at  $x = 0.015$  under a hydrostatic pressure  $P = 15 \text{ kbar}$ . Superconductivity appears as a sharp downturn starting near  $T = 150 \text{ mK}$ . (b)  $\ln(\Delta\rho)$  vs  $\ln T$  where  $\Delta\rho = \rho - \rho_0$  and  $\rho_0$  is the extrapolated zero temperature resistivity. The slope is the power  $n$  in the expression  $\rho(T) = \rho_0 + AT^n$ . (c)  $\rho$  vs.  $T^2$  demonstrating the strong departure of the data from the quadratic temperature dependence that would be expected for a Fermi liquid.

## 8. Summary of compounds in the $\text{ThCr}_2\text{Si}_2$ structure that include Ce, Yb, and U

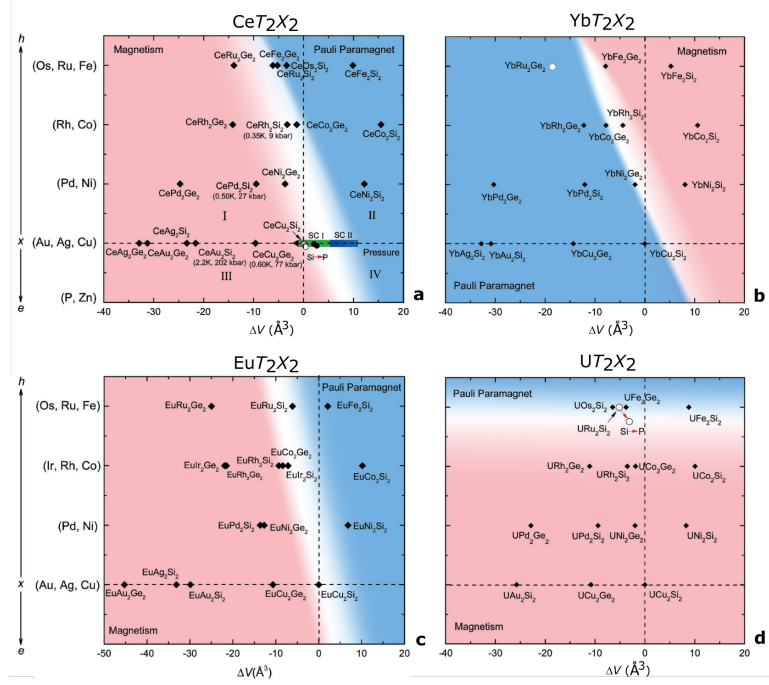


FIG. S8. Two dimensional phase diagrams for the families of compounds (a)  $\text{CeT}_2\text{X}_2$ , (b)  $\text{YbT}_2\text{X}_2$ , (c)  $\text{EuT}_2\text{X}_2$ , and (d)  $\text{UT}_2\text{X}_2$ , ( $T$  = transition metal and  $X = \text{Si, Ge}$ ) that crystallize in the uncollapsed  $\text{ThCr}_2\text{Si}_2$ -type structure. [15–21, 23, 27–31, 46–82] The axes that define the four quadrants (I-IV) and control the ground state behavior are the difference in unit cell volume ( $\Delta V$ ) from that of  $\text{MCu}_2\text{Si}_2$  ( $M = \text{Ce, Yb, Eu, and U}$ ) and hole ( $h$ ) or electron ( $e$ ) doping ( $x$ ). The white band that traverses the phase diagrams separates the magnetic and intermediate valence or Pauli paramagnetic examples. For  $\text{CeT}_2\text{X}_2$ , the detailed information is the same as that presented in the main text. In (b), we note that trivalent Yb is the hole analogue of trivalent Ce, and hence the magnetic and nonmagnetic regions switch position.  $\text{YbRu}_2\text{Ge}_2$  is marked with an open circle because it exhibits an unexpected ordered state at low temperatures that deviates from our expectations. [56] Also presented in (d) are results from the chemical substitution series  $\text{URu}_2(\text{Si}_{1-x}\text{P}_x)_2$ . [83, 84] It is also clear that although Pr and Sm sometimes exhibit unstable valence in other structures, there are no such regions that are easily accessed in the 122 structure (not shown). [85–106] This makes it unappealing to consider these examples for further study.

- 
- [1] N. Mott, in B. Chalmers, Progress in Metal Physics 3, London Pergamon Press, (1952).
  - [2] C. Herring, The State of d Electrons in Transition Metals. *J. Appl. Phys.* **31**, S3 (1960).
  - [3] P. Coleman, C Pépin, Q. Si, and R. Ramazashvili, “How do Fermi liquids get heavy and die?” *Journal of Physics: Condensed Matter* **13(35)**, R723-738 (2001).
  - [4] G. R. Stewart, “Non-Fermi-liquid behavior in *d*- and *f*-electron metals,” *Reviews of Modern Physics* **73(4)**, 797-855 (2001).
  - [5] H. v. Löhneysen, A. Rosch, M. Vojta, and P. Wölfe, “Fermi-liquid instabilities at magnetic quantum phase transitions,” *Reviews of Modern Physics* **79(3)**, 1015-1075 (2007).
  - [6] P. Gegenwart, Q. Si, and F. Steglich, “Quantum criticality in heavy-fermion metals,” *Nature Physics* **4(3)**, 186-197 (2008).
  - [7] C. Pfleiderer, “Superconducting phases of *f*-electron compounds,” *Reviews of Modern Physics* **81(4)**, 1551-1624 (2009).
  - [8] S. Doniach, “The Kondo lattice and weak antiferromagnetism,” *Physica B + C* **91**, 231 (1977).
  - [9] J. Kondo, “Resistance minimum in dilute magnetic alloys,” *Progress in Theoretical Physics* **32**, 37 (1964).
  - [10] M. A. Ruderman and C. Kittel, “Indirect Exchange Coupling of Nuclear Magnetic Moments by Conduction Electrons,” *Physical Review* **96**, 99 (1954).
  - [11] T. Kasuya, “A theory of metallic ferro- and antiferromagnetism on Zener’s model,” *Progress in Theoretical Physics* **16**, 45 (1956).
  - [12] K. Yosida, “Magnetic properties of Cu-Mn alloys,” *Physical Review* **106**, 893 (1957).
  - [13] J. D. Thompson and Z. Fisk, “Progress in Heavy-Fermion Superconductivity: Ce115 and Related Materials,” *Journal of the Physical Society of Japan* **81**, 011002 (2012).
  - [14] K. Gofryk and F. Ronning and J.-X. Zhu and M. N. Ou and P. H. Tobash and S. S. Stoyko and X. Lu and A. Mar and T. Park and E. D. Bauer and J. D. Thompson and Z. Fisk, “Electronic Tuning and Uniform Superconductivity in CeCoIn<sub>5</sub>,” *Physical Review Letters* **109**, 186402 (2012).
  - [15] T. T. M. Palstra, A. A. Menovsky, G. J. Nieuwenhuys, and J. A. Mydosh, “Magnetic properties of the ternary compounds CeT<sub>2</sub>Si<sub>2</sub> and UT<sub>2</sub>Si<sub>2</sub>,” *Journal of Magnetism and Magnetic*

- Materials* **54-57(Part 1)**, 435-436 (1986).
- [16] T. Endstra, G. J. Nieuwenhuys, and J. A. Mydosh, “Hybridization model for the magnetic-ordering behavior of uranium and cerium based 1:2:2 intermetallic compounds,” *Physical Review B* **48(13)**, 9595-9605 (1993).
  - [17] F. Steglich, J. Aarts, C. D. Bredl, W. Lieke, D. Meschede, W. Franz, H. Schäfer, “Superconductivity in the Presence of Strong Pauli Paramagnetism:  $\text{CeCu}_2\text{Si}_2$ ,” *Physical Review Letters* **43(25)**, 1892-1896 (1979).
  - [18] G. Knebel, C. Eggert, D. Engelmann, R. Viana, A. Krimmel, M. Dressel, and A. Loidl, “Phase diagram of  $\text{CeCu}_2(\text{Si}_{1-x}\text{Ge}_x)_2$ ,” *Physical Review B* **53(17)**, 11586-11592 (1996).
  - [19] O. Trovarelli, M. Weiden, R. Müller-Reisner, M. Gómez-Berisso, P. Gegenwart, M. Deppe, C. Geibel, J. G. Sereni, and F. Steglich, “Evolution of magnetism and superconductivity in  $\text{CeCu}_2(\text{Si}_{1-x}\text{Ge}_x)_2$ ,” *Physical Review B* **56(2)**, 678-685 (1997).
  - [20] H. Q. Yuan, F. M. Grosche, M. Deppe, C. Geibel, G. Sparn, and F. Steglich, “Observation of Two Distinct Superconducting Phases in  $\text{CeCu}_2\text{Si}_2$ ,” *Science* **302(5653)**, 2104-2107 (2003).
  - [21] H. Q. Yuan, F. M. Grosche, M. Deppe, G. Sparn, C. Geibel, and F. Steglich, “Non-Fermi Liquid States in the Pressurized  $\text{CeCu}_2(\text{Si}_{1-x}\text{Ge}_x)_2$  System: Two Critical Points,” *Physical Review Letters* **96(4)**, 047008 (2006).
  - [22] A. T. Holmes, D. Jaccard, and M. Miyake, “Valence Instability and Superconductivity in Heavy Fermion Systems,” *Journal of the Physical Society of Japan* **76(5)**, 051002 (2007).
  - [23] F. Steglich, “Heavy-fermion superconductivity in the Kondo-lattice system  $\text{CeCu}_2\text{Si}_2$ ,” *Journal of Physics: Conference Series* **400(Part 2)**, 022111 (2012).
  - [24] T. C. Kobayashi, K. Fujiwara, K. Takeda, H. Harima, Y. Ikeda, T. Adachi, Y. Ohishi, C. Geibel, and F. Steglich, “Valence Crossover of Ce Ions in  $\text{CeCu}_2\text{Si}_2$  under High Pressure Pressure Dependence of the Unit Cell Volume and the NQR Frequency,” *Journal of the Physical Society of Japan* **82(11)**, 114701 (2013).
  - [25] J.-P. Rueff, S. Raymond, M. Taguchi, M. Sikora, J.-P. Itié, F. Baudalet, D. Braithwaite, G. Knebel, and D. Jaccard, “Pressure-Induced Valence Crossover in Superconducting  $\text{CeCu}_2\text{Si}_2$ ,” *Physical Review Letters* **106(18)**, 186405 (2011).
  - [26] K. Miyake, “New trend of superconductivity in strongly correlated electron systems,” *Journal of Physics: Condensed Matter* **19(12)**, 125201 (2007).
  - [27] R. Movshovich, T. Graf, D. Mandrus, J. D. Thompson, J. L. Smith, and Z. Fisk, “Supercon-

- ductivity in heavy-fermion  $\text{CeRh}_2\text{Si}_2$ ,” *Physical Review B* **53**(13), 8241-8244 (1996).
- [28] F. M. Grosche, P. Agarwal, S. R. Julian, N. J. Wilson, R. K. W. Haselwimmer, S. J. S. Lister, N. D. Mathur, F. V. Carter, S. S. Saxena, and G. G. Lonzarich, “Anomalous low temperature states in  $\text{CeNi}_2\text{Ge}_2$  and  $\text{CePd}_2\text{Si}_2$ ,” *Journal of Physics: Condensed Matter* **12**(32), L533-L540 (2000).
- [29] F. M. Grosche, I. R. Walker, S. R. Julian, N. D. Mathur, D. M. Freye, M. J. Steiner, and G. G. Lonzarich, “Superconductivity on the threshold of magnetism in  $\text{CePd}_2\text{Si}_2$  and  $\text{CeIn}_3$ ,” *Journal of Physics: Condensed Matter* **13**(12), 2845-2860 (2001).
- [30] O. Stockert, J. Arndt, E. Faulhaber, C. Geibel, H. S. Jeevan, S. Kirchner, M. Loewenhaupt, K. Schmalzl, W. Schmidt, Q. Si and F. Steglich, “Magnetically driven superconductivity in  $\text{CeCu}_2\text{Si}_2$ ,” *Nature Physics* **7**(2), 119124 (2011).
- [31] Z. Ren, L. V. Pourovskii, G. Girit, G. Lapertot, A. Georges, and D. Jaccard, “Giant Overlap between the Magnetic and Superconducting Phases of  $\text{CeAu}_2\text{Si}_2$  under Pressure,” *Physical Review X* **4**(3), 031055 (2014).
- [32] R. A. Neifeld, M. Croft, T. Mihalisin, C. U. Segre, M. Madigan, M. S. Torikachvili, M. B. Maple, and L. E. DeLong, “Chemical environment and Ce valence: Global trends in transition-metal compounds,” *Physical Review B* **32**(10), 6928-6931 (1985).
- [33] D. D. Koelling and B. D. Dunlap and G. W. Crabtree, “ $f$ -electron hybridization and heavy-fermion compounds,” *Physical Review B* **31**, 4966-4971 (1985).
- [34] B. Buffat and B. Chevalier and M. H. Tulier and B. Lloret and J. Etourneau, “Correlations between structural properties and valence of cerium in  $\text{CeIr}_2\text{Si}_2$ ,” *Journal of Solid State Chemistry* **59**(1), 17-23 (1986).
- [35] V. Vildosola and A. M. Llois and J. G. Sereni, “Influence of  $4f$  hybridization on the structural and electronic properties of  $\text{CeM}_2\text{Si}_2$  ( $M = \text{Ru}, \text{Rh}, \text{and Pd}$ ),” *Physical Review B* **69**(12), 125116 (2004).
- [36] Y. Ikeda, S. Araki, T. C. Kobayashi, Y. Shimizu, T. Yanagisawa, and H. Amitsuka, “A Study of Ni-Substitution Effects on Heavy-Fermion  $\text{CeCu}_2\text{Si}_2$  Similarities between Ni Substitution and High-Pressure Effects,” *Journal of the Physical Society of Japan* **81**(8), 083701 (2012).
- [37] H. Yamaoka, Y. Ikeda, I. Jarrige, N. Tsujii, Y. Zekko, Y. Yamamoto, J. Mizuki, J.-F. Lin, N. Hiraoka, H. Ishii, K.-D. Tsuei, T. C. Kobayashi, F. Honda, and Y. Ōnuki, “Role of Valence Fluctuations in the Superconductivity of Ce 122 Compounds,” *Physical Review Letters*



- 113(8)**, 086403 (2014).
- [38] S. Kambe and S. Raymond and L.-P. Regnault and J. Flouquet and P. Lejay and P. Haen, “Application of the SCR spin fluctuation theory for the magnetic instability in heavy fermion system  $\text{Ce}_{1-x}\text{La}_x\text{Ru}_2\text{Si}_2$ ,” *Journal of the Physical Society of Japan* **65(10)**, 3294-3300 (1996).
  - [39] P. Pedrazzini and M. Gómez Berisso and N. Caroca-Canales and M. Deppe and C. Geibel and J. G. Sereni, “Low temperature magnetic phase diagram of the cubic non-Fermi liquid system  $\text{CeIn}_{3-x}\text{Sn}_x$ ,” *European Physical Journal B* **38**, 445-450 (2004).
  - [40] Y. Luo and J. Bao and C. Shen and J. Han and X. Yang and C. Lv and Y. Li and W. Jiao and B. Si and C. Feng and J. Dai and G. Cao and Z. Xu, “Magnetism and crystalline electric field effect in the  $\text{ThCr}_2\text{Si}_2$ -type  $\text{CeNi}_2\text{As}_2$ ,” *Physical Review B* **86**, 245130 (2014).
  - [41] T. Shang and Y. H. Chen and W. B. Jiang and Y. Chen and L. Jiao and J. L. Zhang and Z. F. Weng and X. Lu and H. Q. Yuan, “Tunable magnetic orders in  $\text{CePd}_2\text{As}_{2-x}\text{P}_x$ ,” *Journal of Physics: Condensed Matter* **26**, 045601 (2014).
  - [42] V. H. Tran and Z. Bukowski, “Ferromagnetism in the Kondo-lattice compound  $\text{CePd}_2\text{P}_2$ ,” *Journal of Physics: Condensed Matter* **26**, 255602 (2014).
  - [43] W. B. Pearson, “The most populous of all crystal structure types – the tetragonal  $\text{BaAl}_4$  structure,” *Journal of Solid State Chemistry* **56(3)**, 278-287 (1985).
  - [44] E. Parthé, B. Chabot, H. F. Braun, and N. Engel, “Ternary  $\text{BaAl}_4$ -type derivative structures,” *Acta Crystallographica Section B* **B39(Part 5)**, 588-595 (1983).
  - [45] I. L. Spain, F. Steglich, U. Rauchschwalbe, H. D. Hochheimer, *Physica B + C* **139-140**, 449 (1986).
  - [46] O. Trovarelli, C. Geibel, M. Grosche, R. Schleser, R. Borth, G. Sparn and F. Steglich, “Low-temperature properties of  $\text{YbCo}_2\text{Ge}_2$ ,” *Physica B* **259-261**, 140-141(1999).
  - [47] O. Trovarelli, C. Geibel, S. Mederle, C. Langhammer, F. M. Grosche, P. Gegenwart, M. Lang, G. Sparn, and F. Steglich, “ $\text{YbRh}_2\text{Si}_2$ : Pronounced Non-Fermi-Liquid Effects above a Low-Lying Magnetic Phase Transition,” *Physical Review Letters* **85(3)**, 626-629 (2000).
  - [48] J. A. Hodges, “Magnetic Ordering of Ytterbium in  $\text{YbCo}_2\text{Si}_2$  and  $\text{YbFe}_2\text{Si}_2$ ,” *Europhysics Letters* **4(6)**, 749-753 (1987).
  - [49] S.K. Dhar, E.V. Sampathkumaran, R. Vijayaraghavan, R. Kuentzler, “ $\text{YbPd}_2\text{Si}_2$ , A moderate heavy fermion system,” *Solid State Communications* **61(8)**, 479-481 (1987)

- [50] G. W. Hull, J. H. Wernick, T. H. Geballe, J. V. Waszczak, and J. E. Bernardini, "Superconductivity in the ternary intermetallics  $\text{YbPd}_2\text{Ge}_2$ ,  $\text{LaPd}_2\text{Ge}_2$ , and  $\text{LaPt}_2\text{Ge}_2$ ," *Physical Review B* **24(11)**, 6715-6718 (1981).
- [51] G. André, P. Bonville, F. Bourée, A. Bombik, M. Kolenda, A. Oleś, A. Pacyna, W. Sikora, A. Szytula, "Magnetic structures of  $\text{RNi}_2\text{Ge}_2$  ( $\text{R} = \text{Dy}, \text{Ho}$  and  $\text{Er}$ ) and  $\text{YbNi}_2\text{Si}_2$ ," *Journal of Alloys and Compounds* **224(2)**, 253-261 (1995).
- [52] C. N. R. Rao, D. D. Sarma, P. R. Sarode, E. V. Sampathkumaran, L. C. Gupta, and R. Vijayaraghavan, "Valence fluctuation in some Yb intermetallics by X-ray photoemission and X-ray absorption," *Chemical Physics Letters* **76(3)**, 413-415 (1980).
- [53] N. D. Dung, T. D. Matsuda, Y. Haga, S. Ikeda, E. Yamamoto, T. Ishikura, T. Endo, S. Tatsuka, Y. Aoki, H. Sato, T. Takeuchi, R. Settai, H. Harima, and Y. Ōnuki, "de Haas-van Alphen Effect and Fermi Surface Properties in High-Quality Single Crystals  $\text{YbCu}_2\text{Si}_2$  and  $\text{YbCu}_2\text{Ge}_2$ ," *Journal of the Physical Society of Japan* **78(8)**, 084711 (2009).
- [54] D. Rossi, R. Marazza, R. Ferro, "Ternary  $\text{rme}_2\text{x}_2$  alloys of the rare earths with the precious metals and silicon (or germanium)," *Journal of the Less-Common Metals*, **66(2)**, P17-P25 (1979).
- [55] A. Grytsiv, D. Kaczorowski, V.-H. Tran, A. Leithe-Jasper, P. Rogl, "Crystal structure and physical properties of Yb-based intermetallics  $\text{Yb}(\text{Cu}, \text{Ag})_2(\text{Si}, \text{Ge})_2$ ,  $\text{Yb}(\text{Cu}_{1-x}\text{Zn}_x)_2\text{Si}_2$  ( $x = 0.65, 0.77$ ) and  $\text{Yb}(\text{Ag}_{0.18}\text{Si}_{0.82})_2$ ," *Journal of Alloys and Compounds*, **504(1)**, 1-6 (2010).
- [56] H. S. Jeevan, C. Geibel, and Z. Hossain, "Quasiquartet crystal-electric-field ground state with possible quadrupolar ordering in the tetragonal compound  $\text{YbRu}_2\text{Ge}_2$ ," *Physical Review B* **73(2)**, 020407(R) (2006).
- [57] P. A. Alekseeva, J.-M. Mignot, K. S. Nemkovski, E. V. Nefedova, V. N. Lazukov, D. Y. Karpunin, R. I. Bewley, A. V. Gribanov, "Magnetic and lattice excitations in intermediate-valence  $\text{EuCu}_2\text{Si}_2$ ," *Physica B* **403(5-9)**, 864-865 (2008).
- [58] Z. Hossain, C. Geibel, H. Q. Yuan and G. Sparn, "Antiferromagnetic transition in  $\text{EuCu}_2\text{Ge}_2$  single crystals," *Journal of Physics: Condensed Matter* **15(19)**, 3307-3313 (2003).
- [59] I. Felner, "Magnetic properties of  $\text{RAu}_2\text{Si}_2$  rare earth compounds," *Journal of Physics and Chemistry of Solids* **36(10)**, 1063-1066 (1975).
- [60] E. Bauminger, I. Felner, D. Froindlich, D. Levron, I. Nowik, S. Ofer, R. Yanovsky, "Mössbauer Effect Studies of Interconfiguration Fluctuations in Metallic Rare Earth Com-

- pounds,” *Journal de Physique Colloques* **35(C6)**, C6-61-C6-70 (1974).
- [61] I. Schellenberg , W. Hermes , S. Lidin , R. Pöttgen, “Structure and properties of the 5.5 K antiferromagnet  $\text{EuAu}_2\text{Ge}_2$ ,” *Zeitschrift fr Kristallographie - Crystalline Materials* **226(3)**, 214-218 (2011).
  - [62] G. Wortmann, I. Nowik, B. Perscheid, G. Kaindl and I. Felner, “Critical evaluation of Eu valences from LIII-edge x-ray-absorption and Mossbauer spectroscopy of  $\text{EuNi}_2\text{Si}_{2-x}\text{Ge}_x$ ,” *Physical Review B* **43(7)**, 5261-5268 (1991).
  - [63] E. V. Sampathkumaran, L. C. Gupta, R. Vijayaraghavan, K. V. Gopalakrishnan, R. G. Pillay and H. G. Devare, “A new and unique Eu-based mixed valence system:  $\text{EuPd}_2\text{Si}_2$ ,” *Journal of Physics C: Solid State Physics* **14(9)**, L237-L241 (1981).
  - [64] Y. Ikeda, A. Mitsuda, N. Ietaka, T. Mizushima, Y. Isikawa, T. Kuwai, “Transport properties under high pressure of antiferromagnet image with unstable Eu valence,” *Journal of Magnetism and Magnetic Materials* **310(2)**, e62-e64 (2007).
  - [65] P. Maślankiewicz, J. Szade, “Valence instability of europium in  $\text{EuCo}_2\text{Si}_2$ ,” *Journal of Alloys and Compounds* **423(1-2)**, 69-73 (2006).
  - [66] B. Chevalier, J. M. D. Coey, B. Lloret and J. Etourneau, “ $\text{EuIr}_2\text{Si}_2$ : a new intermediate valence compound,” *Journal of Physics C: Solid State Physics* **19(23)**, 4521-4528 (1986).
  - [67] Z. Hossain, C. Geibel, “Magnetic properties of single crystal  $\text{EuCo}_2\text{Ge}_2$ ,” *Journal of Magnetism and Magnetic Materials* **264(2-3)**, 142-145 (2003).
  - [68] Z. Hossain, O. Trovarelli, C. Geibel, F. Steglich, “Complex magnetic order in  $\text{EuRh}_2\text{Si}_2$ ,” *Journal of Alloys and Compounds* **323-324**, 396-399 (2001).
  - [69] I. Felner, I. Nowik, “Local and itinerant Magnetism AND Crystal structure of  $\text{RRh}_2\text{Ge}_2$  and  $\text{RRu}_2\text{Ge}_2$  (R = rare earth),” *Journal of Physics and Chemistry of Solids* **46(6)**, 681-687 (1985).
  - [70] A. Prasad, V. K Anand, Z. Hossain, P. L. Paulose and C. Geibel, “Anisotropic magnetic behavior in  $\text{EuIr}_2\text{Ge}_2$  single crystal,” *Journal of Physics: Condensed Matter* **20(28)**, 285217 (2008).
  - [71] L. Chelmicki, J. Leciejewicz, and A. Zygmunt, “Magnetic properties of  $\text{UT}_2\text{Si}_2$  and  $\text{UT}_2\text{Ge}_2$  (T = Co, Ni, Cu) intermetallic systems, ” *Journal of Physics and Chemistry of Solids* **46(5)**, 529-538 (1985).
  - [72] S. P. McAlister, M. Olivier, and T. Siegrist, “Magnetic and electrical properties of  $\text{UCu}_2\text{Ge}_2$ ,”

- Solid State Communications* **69(1)**, 113-116 (1989).
- [73] M. Saran and S. P. McAlister, “Magnetic ordering in the ternary intermetallic compound  $\text{UAu}_2\text{Si}_2$ ,” *Journal of Magnetism and Magnetic Materials* **75(3)**, 345-348 (1988).
  - [74] J. Vejpravová, P. Svoboda, V. Sechovský, C. Ritter, “Evolution of magnetic structures in the  $\text{UNi}_2\text{Si}_2$ - $\text{UPd}_2\text{Si}_2$  system,” *Applied Physics A* **74(Supplement 1)**, s746-s747 (2002).
  - [75] S. B. Roy, A. K. Pradhan, P. Chaddah, “Magnetic properties of polycrystalline  $\text{UNi}_2\text{Ge}_2$ : irreversibility and metastable behaviour,” *Journal of Physics: Condensed Matter* **6(27)**, 5155-5160 (1994).
  - [76] H. M. Duh, I. S. Lyubutin, C. S. Wur, K. J. Lin, J. S. Hwang, C. Tien, and I. J. Chang, “Magnetic phase transitions in  $\text{UPd}_2\text{Ge}_2$ ,” *Journal of Magnetism and Magnetic Materials* **145(3)**, 337-342 (1995).
  - [77] T. Endstra, G. J. Nieuwenhuys, A. A. Menovsky and J. A. Mydosh, “Structural and magnetic properties of  $\text{UCo}_2\text{Ge}_2$ ,” *Journal of Applied Physics* **69(8)**, 4816-4818 (1991).
  - [78] A. Continenza and P. Monachesi, “Magnetization density in  $\text{URu}_2\text{Si}_2$  and  $\text{URh}_2\text{Si}_2$ ,” *Journal of Applied Physics*, **75(10)**, 7027-7029 (1994).
  - [79] A. J. Dirkmaat, T. Endstra, A. A. Menovsky, G. J. Nieuwenhuys and J. A. Mydosh, “Magnetic, Thermal and Transport Properties of  $\text{URh}_2\text{Ge}_2$ ,” *Europhysics Letters*, **11(3)**, 275-280 (1990).
  - [80] T. T. M. Palstra, A. A. Menovsky, G. J. Nieuwenhuys and J. A. Mydosh, “Magnetic properties of the ternary compounds  $\text{CeT}_2\text{Si}_2$  and  $\text{UT}_2\text{Si}_2$ ,” *Journal of Magnetism and Magnetic Materials*, **54-57(Part 1)**, 435-436 (1986).
  - [81] A. Szytuła, M. Slaski, B. Dunlap, Z. Sungaila, A. Umezawa, “Transport and heat capacity properties of  $\text{UFe}_2\text{Si}_2$ ,” *Journal of Magnetism and Magnetic Materials* **75(1-2)**, 71-72 (1988).
  - [82] M. Francois, G. Venturini, J.F. Mareche, B. Malaman, B. Roques, “De nouvelles series de germaniures, isotopes de  $\text{U}_4\text{Re}_7\text{Si}_6$ ,  $\text{ThCr}_2\text{Si}_2$  et  $\text{CaBe}_2\text{Ge}_2$ , dans les systmes ternaires  $\text{RT}_2\text{Ge}_2$  ou R est un element des terres rares et  $\text{T} = \text{Ru}, \text{Os}, \text{Rh}, \text{Ir}$ : supraconductivite de  $\text{LaIr}_2\text{Ge}_2$ ,” *Journal of the Less-Common Metals* **113**, p231-p237 (1985).
  - [83] A. Gallagher, K. W. Chen, C. M. Moir, S. K. Cary, F. Kametani, N. Kikugawa, D. Graf, T. E. Albrecht-Schmitt, S. C. Riggs, A. Shekhter, and R. E. Baumbach, “Unfolding the physics of  $\text{URu}_2\text{Si}_2$  through silicon to phosphorus substitution,” *Nature Communications* **7**, 10712 (2016).

- [84] A. Gallagher, K.-W. Chen, S.K. Cary, F. Kametani, D. Graf, T.E. Albrecht-Schmitt, A. Shekhter, and R. E. Baumbach, “Thermodynamic and electrical transport investigation of  $\text{URu}_2\text{Si}_{2-x}\text{P}_x$ ,” Submitted to *Journal of Physics: Condensed Matter* (2016).
- [85] E. V. Sampathkumaran and I. Das, “Magnetic and electric quadrupolar anomalies in  $\text{PrCu}_2\text{Si}_2$ ,” *Journal of Physics: Condensed Matter* **4**(36), L475-L480 (1992).
- [86] D. Kaczorowski, B. Penc, and A. Szytula, “Thermodynamic and electrical transport properties of  $\text{PrAg}_2\text{Si}_2$ ,” *Journal of Alloys and Compounds* **610**, 428-431 (2014).
- [87] A. Krimmel, J. Hemberger, M. Nicklas, G. Knebel, W. Trinkl, M. Brando, V. Fritsch, A. Loidl, and E. Ressouche, “Spin-glass behavior in  $\text{PrAu}_2\text{Si}_2$ ,” *Physical Review B* **59**(10), R6604-R6607 (1999).
- [88] E. Wawrzyńska, M. Balanda, S. Baran, J. Leciejewicz, B. Penc, N. Stüßer and A. Szytula, “Commensurate-incommensurate magnetic phase transition in  $\text{PrCu}_2\text{Ge}_2$  and  $\text{NdFe}_2\text{Ge}_2$ ,” *Journal of Physics: Condensed Matter* **17**(6), 1037-1047 (2005).
- [89] A. Szytula, M. Balanda, D. Kaczorowski, S. Baran, Ł. Gondek, J. Hernández-Velasco, B. Penc, N. Stüßer, and E. Wawrzyńska, “Magnetic, electronic and transport properties of  $\text{RAg}_2\text{Ge}_2$  ( $\text{R}=\text{Pr}, \text{Nd}$ ) compounds,” *Intermetallics* **14**(3), 315-324 (2006).
- [90] D. A. Joshi, A. K. Nigam, S. K. Dhar, and A. Thamizhavel, “Magnetocrystalline anisotropy in  $\text{RAu}_2\text{Ge}_2$  ( $\text{R} = \text{La}, \text{Ce}$  and  $\text{Pr}$ ) single crystals,” *Journal of Magnetism and Magnetic Materials*, **322**(21), 3363-3371 (2010)
- [91] J. A. Blanco, D. Gignoux, and D. Schmitt, “Specific heat and metamagnetic process in a modulated compound:  $\text{PrNi}_2\text{Si}_2$ ,” *Physical Review B* **45**(5), 2529-2532 (1992).
- [92] V. K. Anand, Z. Hossain, and C. Geibel, “Magnetic properties of  $\text{PrPd}_2\text{Si}_2$  and  $\text{PrPt}_2\text{Si}_2$ ,” *Journal of Physics: Condensed Matter* **19**(48), 486207 (2007).
- [93] R. Welter, G. Venturini, and B. Malaman, “Structural and magnetic properties of the  $\text{ThCr}_2\text{Si}_2$ -type  $\text{PrNi}_2\text{Si}_2$ ,  $\text{PrNi}_2\text{Ge}_2$ ,  $\text{NdNi}_2\text{Si}_2$  and  $\text{NdNi}_2\text{Ge}_2$  compounds,” *Journal of Alloys and Compounds* **329**(1-2), 69-75 (2001).
- [94] R. Welter and K. Halich, “A magnetic study of the  $\text{ThCr}_2\text{Si}_2$ -type  $\text{RPd}_2\text{Ge}_2$  ( $\text{R} = \text{Pr}, \text{Nd}$ ) compounds. Magnetic structure of  $\text{PrPd}_2\text{Ge}_2$  from powder neutron diffraction,” *Journal of Physics and Chemistry of Solids* **67**(4), 862-867 (2006).
- [95] J. K. Yakinthos and Ch. Routsis, “Magnetic structures of  $\text{PrCo}_2\text{Si}_2$  and  $\text{TbCo}_2\text{Si}_2$  structures,” *Journal of Physics and Chemistry of Solids* **45**(6), 689-693 (1984).

- [96] V.K. Anand, Z. Hossain, G. Behr, G. Chen, M. Nicklas, and C. Geibel, “Magnetocrystalline anisotropy and antiferromagnetic phase transition in  $\text{PrRh}_2\text{Si}_2$ ,” *Journal of Physics: Condensed Matter* **19(50)**, 506205 (2007).
- [97] Szytula, J. Leciejewicz, and H. Bińczycka, “Crystal and magnetic structures of  $\text{PrCo}_2\text{Ge}_2$  and  $\text{HoCo}_2\text{Ge}_2$ ,” *Physica Status Solidi A* **58(1)**, 67-70 (1980).
- [98] A. Szytula, D. Kaczorowski, L. Gondek, A. Pikul, A. Arulraj, M. Balanda, S. Baran, and B. Penc, “Magnetic ordering in  $\text{PrT}_2\text{Ge}_2$  ( $T = \text{Ni, Ru, and Rh}$ ) compounds,” *Intermetallics* **18(9)**, 1766-1771 (2010).
- [99] B. Malaman, G. Venturini, A. Blaise, J. P. Sanchez, and G. Amoretti, “Magnetic study of  $\text{PrFe}_2\text{Si}_2$  and  $\text{PrFe}_2\text{Ge}_2$  compounds by susceptibility measurements, neutron diffraction, and Mossbauer spectroscopy,” *Physical Review B* **47(14)**, 8681-8690 (1993).
- [100] J. Vejpravová, J. Proleška, and V. Sechovský, “Magnetic ordering and giant-anisotropy in  $\text{PrRu}_2\text{Si}_2$  and  $\text{PrRu}_2\text{Ge}_2$ ,” *Journal of Magnetism and Magnetic Materials* **316(2)**, e374-e378 (2007).
- [101] N. D. Dung, Y. Ota, K. Sugiyama, T. D. Matsuda, Y. Haga, K. Kindo, M. Hagiwara, T. Takeuchi, R. Settai, and Y. Ōnuki, “Magnetic properties of single crystalline  $\text{RCu}_2\text{Si}_2$  ( $R$ : Rare Earth),” *Journal of the Physical Society of Japan* **78(2)**, 024712 (2009).
- [102] T. D. Matsuda, N. Tateiwa, E. Yamamoto, Y. Haga, and Z. Fisk, “Single crystal growth and magnetic properties of  $\text{SmCu}_2\text{Ge}_2$ ,” *Journal of the Physical Society of Japan* **81(Suppl.B)**, SB037 (2012).
- [103] D. A. Joshi, R. Nagalakshmi, R. Kulkarni, S. K. Dhar, and A. Thamizhavel, “Crystal growth and anisotropic magnetic properties of  $\text{RAg}_2\text{Ge}_2$  ( $R = \text{Pr, Nd, and Sm}$ ) single crystals,” *Physica B* **404(19)**, 2988-2991 (2009).
- [104] S. L. Bud’ko, Z. Islam, T. A. Wiener, I. R. Fisher, A. H. Lacerda, and P. C. Canfield, “Anisotropy and metamagnetism in the  $\text{RNi}_2\text{Ge}_2$  ( $R = \text{Y, La-Nd, Sm-Lu}$ ) series,” *Journal of Magnetism and Magnetic Materials* **205(1)**, 53-78 (1999).
- [105] J. Proleška, J. Vejpravová, and V. Sechovský, “Magnetic and thermodynamic properties of selected  $\text{SmT}_2\text{X}_2$  ternaries,” *Journal of Alloys and Compounds* **408-412**, 359-362 (2006).
- [106] K. Hiebl, C. Horvath, and P. Rogl, M. J. Sienko, “Magnetic properties and structural chemistry of ternary silicides  $(\text{RE, Th, U})\text{Ru}_2\text{Si}_2$  ( $\text{RE} = \text{RARE EARTH}$ ),” *Journal of Magnetism and Magnetic Materials*, **37(3)**, 287-296 (1983).